ASME Journal of Engineering Materials and Technology
Online journal at:
https://asmedigitalcollection.asme.org/materialstechnology

Hyunho Shin[1]
Mechanics of Materials and Design Laboratory,
Department of Materials Engineering,
Gangneung-Wonju National University,
7 Jugheon-ghil,
Gangneung, Gangwon-do 25457, South Korea
e-mail: hshin@gwnu.ac.kr

Sanghoon Kim[1]
Laboratory of Smart Structures and Materials,
Department of Mechanical Design and Engineering,
Chonnam National University,
50 Daehak-ro,
Yeosu, Jeonnam 59626, South Korea
e-mail: shkim83@jnu.ac.kr

Min Kuk Choi
Agency for Defense Development,
P.O. Box 35-5,
Yuseong, Daejeon 34186, South Korea
e-mail: mkchoi87@add.re.kr

Yongwon Ju
Agency for Defense Development,
P.O. Box 35-5,
Yuseong, Daejeon 34186, South Korea
e-mail: joo1@add.re.kr

Extraction of Equivalent Stress Versus Equivalent Plastic Strain Curve of Necking Material in Tensile Test Without Assuming Constitutive Model

An algorithm for extracting the equivalent stress versus equivalent plastic strain curve of a necking material in tensile test is proposed (the curve is called here the equivalent-plastic (EP) stress–strain (SS) curve). The presented algorithm traces the force–elongation curve via iterative finite element (FE) simulations without assuming a constitutive model and is suitable for a general-purpose FE solver available to a general audience. In the FE simulation and experiment, a slightly tapered geometry was employed around the specimen center to stably initiate necking there. The proposed algorithm and mentioned necking initiation method have been applied to extracting the EP SS curve of a high-strength steel material using an axisymmetric specimen. Because necking was initiated stably in simulation at the specimen center for a range of mesh sizes, the convergence of the extracted EP SS curve with the mesh size could be successfully verified. The EP SS curve of the tested material was extracted up to an EP strain of 0.85 with average strain intervals of approximately 2.5 mili-strain. The error values were less than 0.2 and 0.1% after four and seven FE simulations, respectively. The presented algorithm and necking initiation method in simulation can also be used for simultaneously quantifying the fracture EP strain of a necking material in the tensile test. [DOI: 10.1115/1.4064372]

Keywords: constitutive relations, mechanical behavior, plastic behavior

1 Introduction

The majority of general-purpose (commercial) finite element (FE) codes available to a general audience employ J_2 isotropic plasticity theory [1,2] with the von Mises yield criterion. In this theory, the plastic deformation characteristic of a material is described using "equivalent stress" versus "equivalent plastic strain" curve, which is called here the equivalent-plastic (EP) stress–strain (SS) curve for simplicity. The definitions of the related terminologies are available in Sec. S1 available in the Supplemental Materials on the ASME Digital Collection).

The EP SS curve can be measured via the standard tensile test provided the specimen is in the uniaxial stress state. The "standard tensile test" here means the tensile test using a circular- or rectangular bar specimen with a sufficiently long gage-part length together with an extensometer and load cell for measuring specimen elongation and global load, respectively.

Definitions of true stress, true strain, engineering stress, and engineering strain measured in the standard tensile test are also available in the mentioned material. Both the "true" and "engineering" quantities are the "axial" properties measured along the axial direction of the cylindrical specimen (the force-applying direction for a rectangular bar specimen). When we clarify this meaning, "true" stress is interchangeably called here the "axial-true" stress.

In determining the true SS curve of the tensile specimen using Eqs. (S3) and (S4) (see the mentioned material), two assumptions as follows are generally employed for obtaining the current cross-sectional area of the specimen (and subsequently σ):

- While the volume change in the elastic deformation regime is governed by elastic constants, in the plastic deformation regime, the material volume is assumed to be constant.
- The specimen portion bound by the extensometer blades is assumed to deform uniformly (a cylinder shape is maintained for an axisymmetric specimen).

The current cross-sectional area of the specimen (A) can then be obtained using the relationship: $A = A_o L_o / L$, which allows the calculation of σ. The "true" SS curve determined under the above assumptions has the following two characteristic features:

- In the work-hardening regime of the axial-true SS curve, the earlier assumptions are generally valid, and thus, the measured curve in this regime is reliable as the physical property of the specimen material. Furthermore, the stress state is uniaxial,

[1]Corresponding authors.

Contributed by the Materials Division of ASME for publication in the Journal of Engineering Materials and Technology. Manuscript received September 9, 2023; final manuscript received December 7, 2023; published online January 22, 2024. Assoc. Editor: Ankit Srivastava.

and thus, the measured "true" SS curve is identical to the EP SS curve.
- Once the axial force reaches the maximum value and decreases thereafter toward fracture, the specimen no longer deforms uniformly as a cylinder but necking occurs, and thus, the measured "true" SS curve in the post-necking regime cannot be regarded as a physical property of the specimen material. Furthermore, the stress state in the neck region becomes a multiaxial stress state, and thus, the "true" SS curve is no longer the EP SS curve.

Therefore, extracting the EP SS curve in the post-necking regime is fundamental and important because the extracted curve can serve as a property of the material [3] in the framework of the J_2 plasticity theory; the extracted curve can be used as a mean for comparison with other materials. The extracted EP SS curve is also essential for precisely calibrating the constitutive model [4–9], which is indispensable for the simulation of the mechanical deformation behavior of solids and structures. (The EP SS curve itself can also be regarded as the constitutive model.)

As will be reviewed in Sec. 2, a number of studies pursued the extraction of the EP SS curve, especially in the post-necking regime by either analytically correcting the measured true SS curve [10–18] or inversely tracing (constructing) the tensile test result [19–47] (e.g., the force–elongation curve) via iterative FE simulations. Here, this method is called the inverse method. The majority of the inverse method studies [19–40] assumed a constitutive model in the iterative FE simulations. Only a few of the inverse studies [41–47] extracted the EP SS curve without assuming a constitutive model.

This study focuses on the inverse method of extracting the EP SS curve without assuming a constitutive model. As will be reviewed in Sec. 2, existing algorithms for this purpose are unsuitable for a general-purpose FE solver, which is available to a general audience. Furthermore, as will be discussed later (Sec. 4.5), previous inverse studies and related works employed geometrically perfect FE models (without geometrical flaws) [19–47]. To the best of our knowledge, no inverse studies explicitly demonstrated the convergence of the extracted EP SS curve over a range of mesh sizes, probably because necking could not be stably obtained for varying mesh sizes in the geometrically perfect FE models.

This paper therefore aims to develop an efficient and suitable algorithm for a general-purpose FE solver to extract the EP SS curve without assuming a constitutive model. In the FE simulation and experiment, a slightly tapered geometry was employed around the specimen center to stably initiate necking there, which allowed us to verify the convergence of the EP SS curve over a range of mesh sizes; the converged curve was extracted as the solution curve according to the presented algorithm.

2 Literature Survey

2.1 Categorization of EP SS Curve Extraction Method

2.1.1 Analytical Correction Method. In this method, analytical equations are applied to correct the current cross-sectional area in the post-necking regime; the experimentally measured axial-true SS curve under the cylinder model assumption is eventually corrected. The Bridgman equation [10–13] is the most famous analytical correction equation for a circular bar specimen. A Bridgman equation-independent correction method using a round notched circular bar specimen [14] and correction equations for rectangular bar specimens [15–18] were also developed. Because the stress state of the necked region notably deviates from the uniaxial stress state after the onset of necking, the analytically corrected axial-true SS curve generally needs to be corrected further to obtain the EP SS curve by considering the stress state of the necked volume. There may be cases where the analytically corrected true SS curve was consistent with the EP SS curve. However, as pointed out in Ref. [43], the validity and relevance of the mentioned consistency for other materials are still unclear because the constitutive model employed in checking the consistency is generally dependent on the material. Furthermore, the empirical parameters of the analytical equations would also be dependent on the material.

2.1.2 Inverse Method. The inverse method resorts to an inverse engineering process to construct (simulate or trace) the target (e.g., measured quantities such as the force–elongation curve) via iterative simulations under assumed EP SS curves (or assumed constitutive parameters if a constitutive model is employed). In this method, the objective function is defined, which is a non-dimensional formulation quantifying the difference between the target and simulated counterpart. The EP SS curve (or the constitutive parameters) inputted to the FE simulation when the target was reasonably simulated is extracted as the solution. The inverse method can also be applied to tests under different stress states such as the compression test [49] and shear test [50].

The inverse method for the tensile test is not limited to the standard specimens such as circular and rectangular bar specimens. Non-standard specimens like the round notched axisymmetric specimen can also be used. Because whether or not the standard tensile specimen is used is not essential in extracting the EP SS curve in the inverse approach, the specimen type is not used here as a reference for categorizing the method of EP SS curve extraction. However, this work prefers a specimen geometry as close as that of the standard specimen (with a circular or rectangular cross section) without an overly apparent notch because (i) the extracted EP SS curve from the specimen with a larger volume is more reliable and (ii) a simple geometry is favorable for minimizing machining deviation.

In the inverse method under an assumed constitutive model [19–40], as mentioned, the constitutive parameters are updated in the iterative FEA process. In the method without assuming a constitutive model [41–47], the equivalent stress values at a range of EP strain steps are directly updated. The error of the latter is generally lower than the errors of the former and the analytical correction method. It is therefore desirable to reserve a sure (infallible) EP SS curve first via the inverse method without assuming a constitutive model. Then, modeling of the reserved curve is to be followed next depending on necessity.

2.2 Notation and Terminology for Inverse Method Studies

2.2.1 Notation. In the stream of research [24,41–47] that this work belongs to, elongation (δ) steps are generally predefined. In this paper, the superscript i denotes the index of the elongation (δ) step. Thus, δ^i indicates the elongation value (δ) at the ith predefined step. The elongation index i is also used as the superscript to note the corresponding quantities (e.g., F^i, ε^i, $\bar{\varepsilon}^i$, σ^i, and $\bar{\sigma}^i$) at a given elongation step i. Another superscript j is the FEA index in our algorithm (In the previous algorithm [24,41–47], j is the stress update index at a given elongation index i.). Thus, for instance, here, $\bar{\varepsilon}^{i,j}$ denotes the $\bar{\varepsilon}$ value when δ reaches δ^i in the jth FE simulation.

2.2.2 Terminology. To the best of our knowledge, Zhano and Li [41] were pioneers in extracting the EP SS curve via the inverse method using iterative FE simulations. They used an in-house code and claimed to have extracted the "stress–strain" curve from a necking material, which was somewhat a loose terminology. The succeeding inverse method study was carried out by Ling [19] using a general-purpose FE code (ABAQUS). Ling [19] claimed to have extracted the "true stress" and "true strain" from a necking material. Since then, later inverse studies called the extracted quantities from the necking material "stress" and "strain" [22,47], "true stress" and "true strain" [23–32], "stress" and "true plastic strain" [45], "yield stress" and "effective plastic strain" [33], "effective stress" and "effective strain" [34,46], and "equivalent stress" and "equivalent plastic strain" [20,21].

The general-purpose FE solvers request the user to input the plastic part of the equivalent SS curve (i.e., the EP SS curve)

separately from the elastic part (which is inputted using two elastic constants such as the elastic modulus and Poisson's ratio). Although a series of trial sets of axial-true plastic SS data, i.e., (ε^i, σ^i) data, are inputted to FEA, the FE solver based on J_2 plasticity theory regards the inputted (ε^i, σ^i) data as the ($\bar{\varepsilon}^i$, $\bar{\sigma}^i$) data (i.e., the EP SS data). Therefore, unless the authors made the procedure unnecessarily complicated by manipulating the general-purpose code, the inputted (ε^i, σ^i) set for the plastic deformation regime when the error between F^i_{exp} and F^i_{sim} was minimized played the role of the ($\bar{\varepsilon}^i$, $\bar{\sigma}^i$) set in the FE simulation; what was finally extracted in the inverse method was the EP SS curve rather than the "axial-true" SS curve. Therefore, we assume that the above studies actually extracted the EP SS curve (unless otherwise specified) and thus the notations for EP SS data ($\bar{\varepsilon}^i$, $\bar{\sigma}^i$) are used here when we review the related studies in the next sections.

In a later study, if necking occurs in the specimen and J_2 plasticity theory with the von Mises yield criterion is employed in the iterative FE simulations, it is desirable to use the exact terminologies for the extracted quantities: "equivalent stress" and "equivalent plastic strain" (or "effective stress" and "effective plastic strain"). If necking does not occur during plastic deformation, the extracted quantities via the iterative FEA can be interchangeably called the "true stress" and "true plastic strain."

2.3 Critical Review of Inverse Method Studies

2.3.1 Studies Without Assuming Constitutive Model. The studies on the inverse method without assuming a constitutive model and related works are critically reviewed in the Supplemental Material (Sec. S2 available in the Supplemental Materials on the ASME Digital Collection). The summary of the review is as follows.

In the study of Zhano and Li [41], strain steps were not predefined in the post-necking regime (unlike in the pre-necking regime) and thus both the strain and stress had to be searched for in the open space of ($\bar{\varepsilon}^i$, $\bar{\sigma}^i$) in the post-necking regime. This feature imposed an overly high computational burden [19]. Furthermore, no referable algorithm for the post-necking regime was available in their study.

Conversely, Joun et al. [24] disclosed a detailed algorithm for extracting the EP SS curve. To the best of our knowledge, they were the first who searched for only one variable ($\bar{\sigma}^i$) at predefined $\bar{\varepsilon}^i$ values (when δ_{sim} reached $\delta^i = \delta^i_{exp}$) in the post-necking regime instead of searching for both $\bar{\varepsilon}^i$ and $\bar{\sigma}^i$. Furthermore, Joun et al. were the first who used a stress update equation instead of monotonically searching for stress ($\bar{\sigma}^i$). Because of the one-variable search character and stress update equation, their algorithm should have significantly reduced the computational burden of the previous study [41].

However, as will be presentd later (Sec. 3.3), their method was eventually dependent on the employed constitutive model. Furthermore, to implement their algorithm using a general-purpose FE solver, techniques like the restart option need to be employed, which is still computationally demanding. Nevertheless, the framework of their algorithm was transferred to a number of later studies [43–45], which did not assume constitutive models and employed general-purpose solvers. Some points to be desired in the mentioned later studies [43–45] are reviewed in the mentioned supplemental material from the viewpoint of algorithm rigorosity.

As for other studies that employed the general-purpose solvers, the detailed procedures of EP SS curve extraction in the studies by Tao et al. [46] and Tardif and Kyriakides [47] were unavailable. The concept of the EP SS curve extraction in the study by Chu [42] needed to be manifested on a quantitative base.

2.3.2 Studies Under Assumed Constitutive Model. The plastic part of the force–elongation curve originates directly from the EP SS curve of a plastically deforming material. The former is actually the most informative source from which the EP SS curve can be straightforwardly extracted, as can be observed in the standard tensile test. Consequently, not only the inverse studies without assuming a constitutive model [41–47] but also the majority of the studies under assumed constitutive models [19–34] employed the force–elongation curve in the objective function. However, the accuracy of the extracted EP SS curve under an assumed constitutive model relies on the accuracy of the employed constitutive model, which is essentially dependent on the material type. Furthermore, the constitutive model often unsuccessfully describes the flow (equivalent) stress especially near the fracture strain [36].

Because the digital image correlation (DIC) technique accurately characterizes the displacement field on the specimen surface, the displacement field (DIC data) has also been actively employed in the objective function [35–40]. To the best of our knowledge, all of the inverse method studies that employed the DIC data (displacement field) assumed a constitutive model in the iterative FEA process and thus were exposed to the mentioned drawbacks of assuming a constitutive model.

The studies that employed the DIC data are critically reviewed in the supplemental material from the viewpoint of the objective function (or target to be traced). As reviewed therein, it is desirable to include the force–elongation data in the objective function or use it at least as a tool to verify the result of employing only the DIC data. The combination of the DIC data (displacement field) with the force–elongation curve in the objective function would contribute to verifying the cost-effectiveness of the force–elongation curve in extracting the EP SS curve. As will be presented later (Sec. 4.1), this study, which utilizes the force–elongation curve in the objective function, routinely results in a few hundred data points on the extracted EP SS curve without assuming a constitutive model. Conversely, for the DIC data in an objective function to yield such a number of data points on the extracted EP SS curve under an assumed constitutive model, a much higher computational burden needs to be paid.

3 Proposed Algorithm

3.1 Characteristic Features. To more clearly explain the proposed algorithm, the notation for the EP SS curve, i.e., $\bar{\sigma}^{i,j}(\bar{\varepsilon}^{i,j})$, is divided here into $\bar{\sigma}^{i,j}_{input}(\bar{\sigma}^{i,j}_{input})$ and $\bar{\sigma}^{i,j}_{output}(\bar{\sigma}^{i,j}_{output})$. The former denotes the inputted EP SS curve to the FE simulation, and the latter indicates the outputted EP SS curve from the representative element in the neck region in the FE simulation.

In a number of inverse method studies [24,43–45] the stress was iteratively updated first at a given δ^i (or $\bar{\varepsilon}^i$) step, i.e., at a given elongation index *i:* the stress-updating loop (j index-varying loop) was the inner loop at a given elongation index i. Then, the stress-updating loop was repeated for all δ^i (or $\bar{\varepsilon}^i$) steps (the loop that changed elongation index i was the "outer" loop).

The first characteristic feature of the proposed algorithm here is that the loop that changes the elongation index i is the "inner" loop: after a given FEA (index j), the stress update at each δ^i step is repeated for all elongation indexes. Then, the next FEA is carried out (the loop that changes the FEA index j is the outer loop). Such a feature should be more appropriate for a general-purpose FE code than the previous algorithm because the stress update is carried out for all i indices (inner loop) in the post-processing stage after each FEA cycle (jth cycle in the outer loop) is completed.

The second feature of the presented algorithm is that a constitutive-model-independent stress update "equation" is employed, which is presented later in Eq. (1). It is different from the constitutive-model-dependent form (see Eq. (S7) in Sec. S2 available in the (Supplemental Materials on the ASME Digital Collection).

The final feature is that a new stress update "factor", named the fraction-based factor ($U_f = (F_{sim} - F_{exp})/F_{exp}$), is presented. This

factor is used here together with the ratio-based update factor ($U_r = F^i_{exp}/F^i_{sim}$) available in Ref. [24].

3.2 Procedures. The following describes the algorithm developed here (see Fig. 1).

(Step 1) Predefine δ^i steps on the measured $F_{exp}(\delta_{exp})$ curve. The elongation is measured between the two predefined probe positions on the specimen surface using, e.g., an extensometer (or DIC instrument). The global force is measured using a load cell.

(Step 2) Input appropriate axial-true SS curve as the initially guessed EP SS curve to the first FEA. (Examples of the methods of guessing the initial EP SS curve will be presented in Sec. 4.3.)

(Step 3) Carry out the jth FEA up to the $\delta^{max}(=\delta^{max}_{exp}=\delta^{max}_{sim})$ value. In the post processing stage, extract the time histories of force and elongation from the output database (ODB) file. Determine $F^{i,j}_{sim}(\delta^{i,j}_{sim})$ points whenever δ^j_{sim} reaches predefined δ^i values. After the elongation-step loop (i loop) is completed, calculate the overall error of the $F^{i,j}_{sim}(\delta^i)$ curve with reference to the $F^i_{exp}(\delta^i)$ curve. If the calculated overall error is within the predefined value, stop the FEA (terminate the j loop for the FEA iteration); the EP SS curve inputted to the current FEA is the determined EP SS curve via the current algorithm. Otherwise, extract the time histories of equivalent stress and EP strain from the current (jth) simulation result (ODB file) and determine $\bar{\sigma}^{i,j}_{output}(\bar{\varepsilon}^{i,j}_{output})$ points whenever δ^j_{sim} reaches a predefined δ^i. Set $\bar{\varepsilon}^{i,j+1}_{input} = \bar{\varepsilon}^{i,j}_{output}$ for inputting to the next FEA. Then, update the stress using the equation:

$$\bar{\sigma}^{i,j+1}_{input} = \bar{\sigma}^{i,j}_{output} \times U \tag{1}$$

where U is the stress update factor, which will be described below. Set $j=j+1$ and go to Step 3 for the next FEA which utilizes the $\bar{\sigma}^{i,j+1}_{input}(\bar{\varepsilon}^{i,j+1}_{input})$ curve as the input EP SS curve (the end of the overall algorithm description).

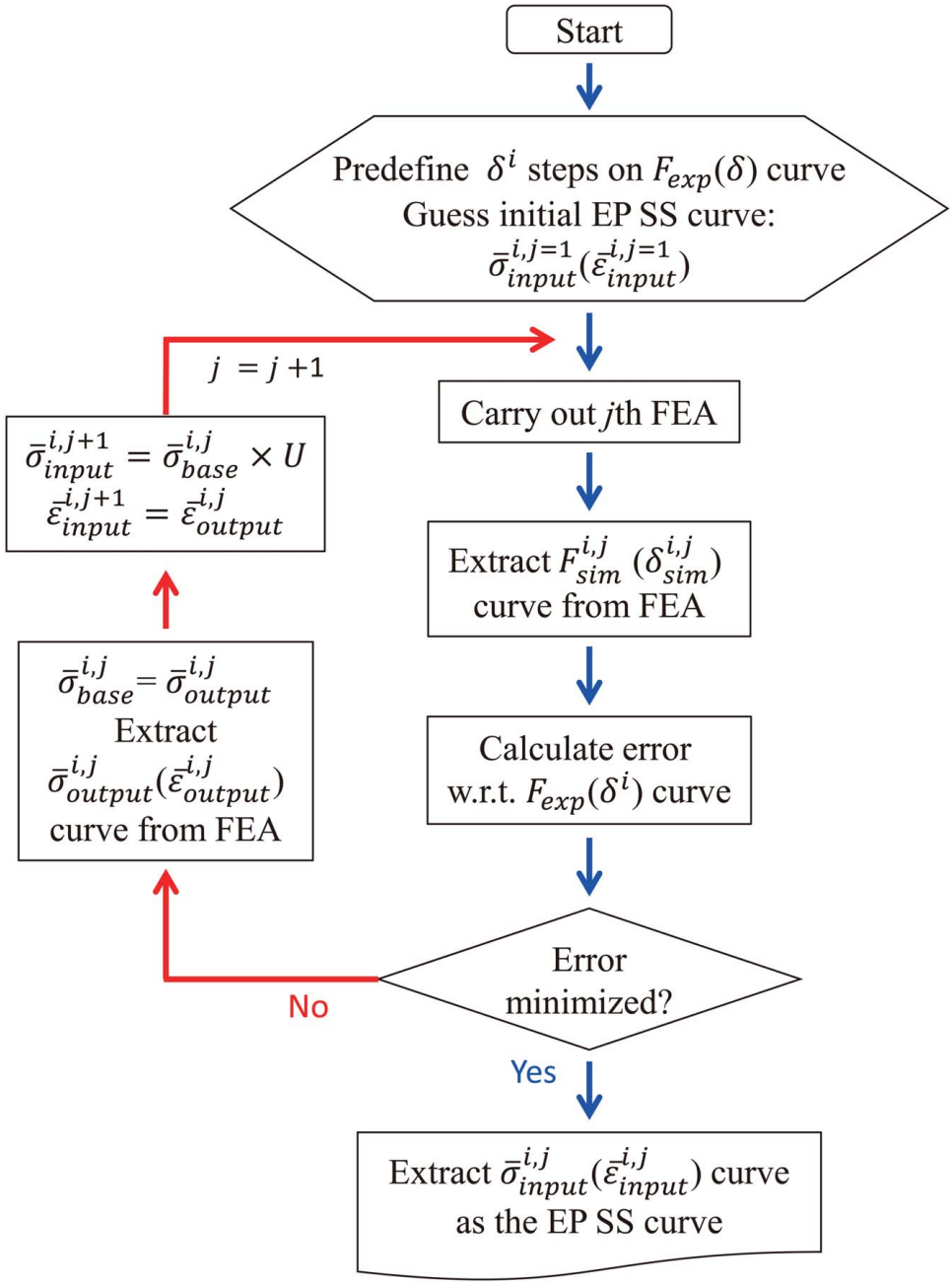

Fig. 1 Flowchart of the proposed algorithm

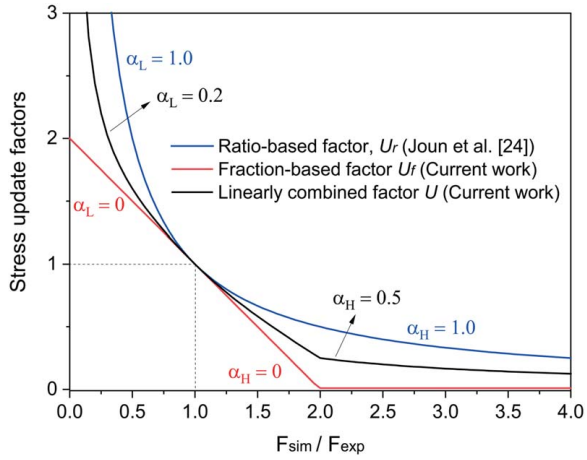

Fig. 2 Linear combination of the fraction-based stress update factor (U_f) with the ratio-based one (U_r)

In Eq. (1), the stress update factor (U) is the linear combination of the ratio-based update factor (U_r) and the fraction-based update factor (U_f). The ratio-based update factor (U_r) was introduced by Joun et al. [24]

$$U_r = F^i_{exp}/F^i_{sim} \tag{2}$$

and the fraction-based update factor (U_f) introduced here is

$$U_f = (1 - [F^i_{sim} - F^i_{exp}]/F^i_{exp}) = (2 - F^i_{sim}/F^i_{exp}) \quad \text{for } 0 < F^i_{sim}/F^i_{exp} < 2 \tag{3}$$

$$U_f = 0.01 \text{ for } F^i_{sim}/F^i_{exp} \geq 2 \tag{4}$$

The linearly combined update factor (U) is then

$$U = U_f + \alpha_L(U_r - U_f) \text{ for } F^i_{sim}/F^i_{exp} < 1 \tag{5}$$

$$U = U_f + \alpha_H(U_r - U_f) \text{ for } F^i_{sim}/F^i_{exp} > 1 \tag{6}$$

where $\alpha_L(0 \leq \alpha_L \leq 1)$ and $\alpha_H(0 \leq \alpha_H \leq 1)$ are the parameters independently controlled by the user. Their roles are illustrated in Fig. 2.

In our algorithm, the error between the overall curves of the target (experiment) and the simulation is calculated using the equation:

$$\text{Error}(\%) = \frac{\int_0^{\delta^{max}} |F_{sim} - F_{exp}| d\delta}{\int_0^{\delta^{max}} F_{exp} d\delta} \times 100 \tag{7}$$

which is the percentage of the absolute area difference between the two curves ($F_{sim}(\delta_{sim})$ and $F_{exp}(\delta_{exp})$) with reference to the area of the target curve $\left(\int_0^{\delta^{max}} F_{exp} d\delta\right)$. Equation (7) is the objective function to be minimized in the current algorithm.

3.3 Base Stress for Update. The term "base stress" is defined here as the target to be multiplied by an update factor (U) in a stress update equation. In Eqs. (1) and (S7), the base stresses are $\bar{\sigma}^{i,j}_{output}$ and $\bar{\sigma}^{i,j}_{interpol}$, respectively. To expound their characteristics, Fig. 3 illustrates their values at $\bar{\varepsilon}^{i,j}_{output}$ (for the jth FEA). Figure 3 also plots the reference curve, which was created in Ref. [24] by fitting the measured true SS curve using the Hollomon constitutive model. In Ref. [24], the reference curve was the initially guessed EP SS curve for inputting to the first FEA. As can be observed in Fig. 3, the $\bar{\sigma}^{i,j}_{interpol}$ value is limited to a point on the reference curve while the $\bar{\sigma}^{i,j}_{output}$ value varies freely depending on the output of the jth FEA. Because $\bar{\sigma}^{i,j}_{output}$ is generally closer to the final solution than $\bar{\sigma}^{i,j}_{interpol}$, it is desirable to employ $\bar{\sigma}^{i,j}_{output}$ as the base stress, which should allow the program to reach the final solution in fewer FEA iterations.

In case $\bar{\sigma}^{i,j}_{interpol}$ is employed as the base stress, as mentioned, the stress values on the same reference curve (but at different strain values) are continually inputted to the stress update equation. This feature will partially nullify the efficiency of the update factor and will eventually increase the number of stress update cycles. In Ref. [24], 300 FE simulations were required to reach the final solution curve with approximately ten data points. However, as will be shown later in Sec. 4, we reached the solution curve with 350 data points with less than 0.2% and 0.1% of error in four and seven FE simulations, respectively, by using $\bar{\sigma}^{i,j}_{output}$ as the base stress for stress update.

In that the $\bar{\sigma}^{i,j}_{interpol}$ values determined on the Hollomon-model-determined curve (reference curve) were continually inputted to the stress update, the previous algorithm [24] was eventually constitutive-model dependent. Conversely, the stress update algorithm here, which employs $\bar{\sigma}^{i,j}_{output}$ as the base stress, is completely independent of any constitutive model. (The firstly inputted EP SS curve to the FEA is open to the user.)

3.4 Stress Update Factor and Algorithm (Equation). Revisit Fig. 2 which illustrates stress update factor (U) that linearly combines the ratio-based factor (U_r) and fraction-based factor (U_f). In usual cases where the initially guessed EP SS curve is appropriately selected so that $F_{sim}/F_{exp} \approx 1$ from the first FEA, selecting purely $U_r(\alpha_L = \alpha_H = 1)$ or purely $U_f(\alpha_L = \alpha_H = 0)$ does not practically matter: both factors should result in very similar stress paths at a given EP strain in reaching the final solution (equivalent stress).

Nevertheless, the algorithm here copes with the case where $F_{ratio}(= F_{sim}/F_{exp}) < 1$ (see Fig. 2). In this F_{ratio} regime, U_r overly increases toward infinity as F_{ratio} decreases. Then, the stress can be over-updated. Conversely, U_f increases moderately as F_{ratio} decreases; the chance of a stress over-update would be diminished. Therefore, for step-by-step correction of the stress with a diminished over-update, one can employ $U_f(\alpha_L = 0)$ when $F_{ratio} \leq 1$. When $F_{ratio}(= F_{sim}/F_{exp}) > 1$, U_r is closer to unity than U_f and thus $U_r(\alpha_H = 1)$ may be advantageous for a step-by-step update of the stress.

Even when the purely ratio-based stress update "factor" (U_r) is employed over the entire F_{ratio} range ($\alpha_L = 1$ and $\alpha_H = 1$), the stress update "algorithm" (or equation; Eq. (1)) here should not be considered to be the same as the previous one because the

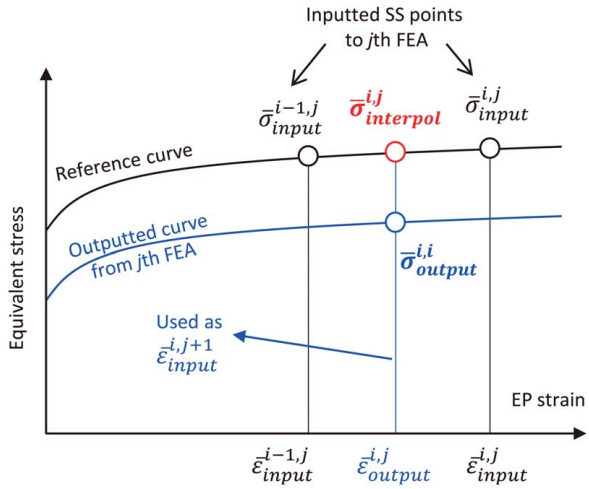

Fig. 3 Comparison of the base stress determination method here ($\bar{\sigma}^{i,j}_{output}$) with that of Joun et al. [24] ($\bar{\sigma}^{i,j}_{interpol}$), both when δ_{sim} reaches δ^i. Vertical lines indicate the traces of the iso-strain.

base stress here ($\bar{\sigma}^{i,j}_{output}$ in Eq. (1)) is different from Ref. [24] ($\bar{\sigma}^{i,j}_{interpol}$); the amount (degree) of update is different at each stress update.

4 Example of Extracting EP SS Curve

4.1 Experiment. This study pursued a simple, inexpensive, and yet reliable characterization method; the measured axial force–elongation curve, $F_{exp}(\varepsilon_{exp})$, was employed as the target to be traced in the iterative FE simulations. This work avoided employing the curve measured using a DIC instrument because the ε_{exp} value is dependent on the speckle distance [51].

The steel material used here was received from Poongsan Co. (Control No. 2206-BM7C1; Angang, Gyungbuk, South Korea). The axisymmetric geometry of the prepared tensile specimen is illustrated in Fig. 4(*a*), together with its FE model in Fig. 4(*b*) and the finally deformed shapes in the tensile test and FEA (Fig. 4(*c*)).

To stably induce necking at the specimen center, the central portion of the specimen ($-10 \le y \le 10$ mm) was machined to be slightly tapered: the diameter at the specimen center ($y = 0$) was 6.90 mm while it was 6.96 mm at $y \ge \pm 10$ mm. The two extensometer blades (not shown) were positioned at $y = \pm 12.5$ mm. The tensile test was carried out using a universal material tester (Model 322, MTS Systems Corporation, Eden Prairie, MN) at a nominal crosshead speed of 3 mm/min. Two blades (steel) of the extensometer were glued to the specimen using an adhesive, which was suitably removed using acetone after the experiment.

The measured force–elongation curve is presented in Fig. 5(*a*), where the average elongation interval was 0.01 mm (349 data intervals up to the fracture elongation of 3.49 mm). To calculate the axial-true SS curve from Fig. 5(*b*), a hypothetical cylinder specimen was assumed: its length was 25 mm (which corresponds to the extensometer length), and its diameter was 6.936 mm (which was the average specimen diameter between the two extensometer blades). Then, σ and ε were calculated using Eqs. (S3) and (S4) (Sec. S1 available in the Supplemental Materials on the ASME Digital Collection), respectively. As mentioned, the current cross-sectional area (A) in the foregoing equations is obtained by assuming the "volume constancy" of the "cylindrical" specimen during plastic deformation ($A = A_o L_o / L$). The origin of the strain (work) softening phenomenon observed in Fig. 5(*a*) (after the maximum point on the axial-true SS curve) is discussed later (Sec. 4.4. "Solution Finding Process") in contrast with the finally extracted EP SS curve. The axial-engineering SS curve was calculated using Eqs. (S5) and (S6), and the result is also presented in Fig. 5(*b*).

4.2 Finite Element Analysis. Finite element analysis of the tensile test was carried out using ABAQUS Standard [52] as the solver (implicit analysis). A quarter of the two-dimensional axisymmetric specimen area was modeled considering the symmetry of the specimen (Fig. 4(*b*)). The model area was discretized using four-node bilinear axisymmetric quadrilateral (reduced integration and hourglass control) elements (CAX4R). The y-displacement of the nodes at the bottom of the FE model was fixed, and that of the nodes at the grip part of the FE model was controlled.

As the elastic properties of the specimen, a Poisson's ratio of 0.29 was adapted from the literature for carbon steel [53]. The elastic modulus value (199.95 GPa) was separately verified via the trial FE simulations of the force–elongation curve for a range of elastic modulus values (not shown). For the first FE simulation in the iterative FEA process, an initially guessed EP SS curve was inputted to describe the plastic deformation behavior of the specimen. The process of preparing the foregoing curve is described in Sec. 4.3.

After each FEA, the time histories of necessary variables were outputted to the output database (ODB) file. The reaction force (RF2) of the top nodes and the displacement (U2) of the node initially at $y = 12.5$ mm ($r = 0$) were outputted. The equivalent stress (MISES) and plastic equivalent strain (PEEQ) of the element

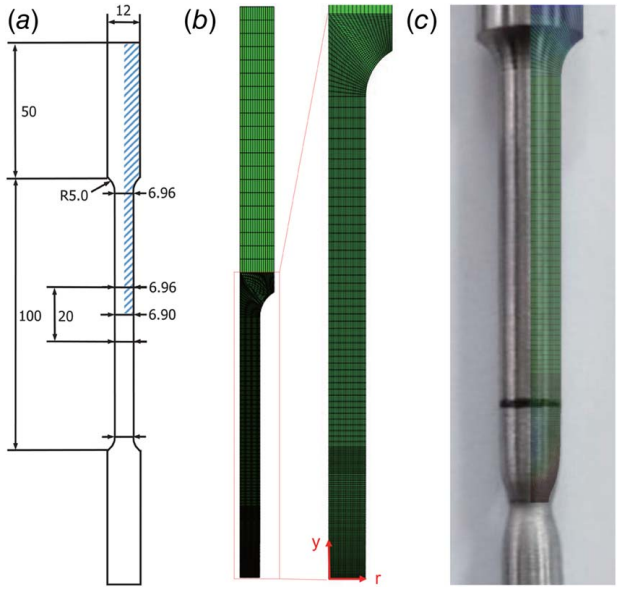

Fig. 4 (*a*) Geometry of the tensile specimen. The hatched area in (*a*) was discretized as the axisymmetric FE model, which is in (*b*). (*c*) Comparison of the finally deformed shape of the neck region in the experiment with the simulation result.

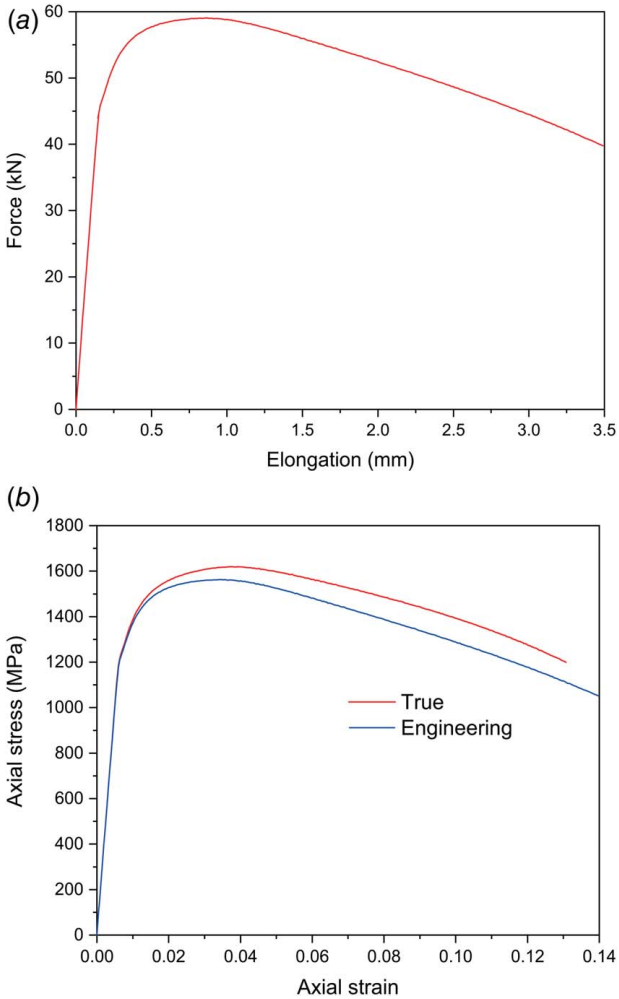

Fig. 5 (*a*) Force–elongation curve measured from the tensile test and (*b*) axial stress–strain curves

closest to the origin of the FE model were also outputted as the representative quantities in the neck.

The time histories of the foregoing variables were extracted from the ODB file using a program written in PYTHON. The RF2 values of the top nodes were summed while the U2 value was multiplied by two to match the values of the experimental counterparts. (The summed and multiplied values are still assigned to the same notations of RF2 and U2, respectively, in the following.) Then, the four variable values (RF2, MISES, PEEQ, and U2) were linearly interpolated to obtain the values when U2 reached predefined δ^i values. The interpolated values are noted here as $F_{sim}^{i,j}$, $\bar{\sigma}^{i,j}$, $\bar{\varepsilon}^{i,j}$, and $\delta^{i,j}(=\delta^i)$, respectively.

4.3 Initial EP SS Curve. The pre-necking part of the axial-true SS curve (Fig. 5(*b*)) was used to calibrate the Voce model: $(\bar{\sigma} = A + B[1 - \exp(-C\bar{\varepsilon})])$. The calibrated Voce-model-predicted curve is illustrated in Fig. 6, which was employed here as the initial EP SS curve to be inputted into the first FE simulation. To prepare the initial EP SS curve by modeling the pre-necking part of the axial-true SS curve, other relevant models, e.g., the Ludwik model $(\bar{\sigma} = A + B\bar{\varepsilon}^n)$, Hollomon model $(\bar{\sigma} = k\bar{\varepsilon}^n)$, or the linear combination of the Hollomon and linear models [19], can also be employed depending on the choice of the user.

4.4 Solution Finding Process. This section explains the solution-curve-finding process using the FE mesh shown in Fig. 4(*b*). The number of meshes was 32 along the radial direction (at $y = 0$). The progress of the target tracing process with the iterations of FEA is illustrated in Fig. 7(*a*). The EP SS curves inputted to the FE simulations in the target tracing process are shown in Fig. 7(*b*). In Fig. 7(*a*), the force–elongation curves after the fourth ($j = 4$) and seventh ($j = 7$) FE simulations showed error values of less than 0.2% and 0.1%, respectively, with reference to the experimental counterpart. The EP SS curve inputted to the seventh FEA ($j = 7$) in Fig. 7(*b*) was arbitrarily determined here as the solution curve.

Note in Fig. 7(*b*) that the initial EP SS curve ($j = 1$) was inputted to the first FE simulation. According to our algorithm (Sec. 3), the $\bar{\varepsilon}_{sim}$ value when δ_{sim} reached 3.49 mm in the first FE simulation is the maximum strain in the inputted EP SS curve for the second FEA ($j = 2$). Likewise, the final $\bar{\varepsilon}_{sim}$ in the second FEA (when δ_{sim} reached 3.49 mm) is the maximum strain of the inputted EP SS curve for the third FEA ($j = 3$). As can be observed in Fig. 7(*b*), the maximum EP strains when δ_{sim} reached 3.49 mm are different depending on the j value.

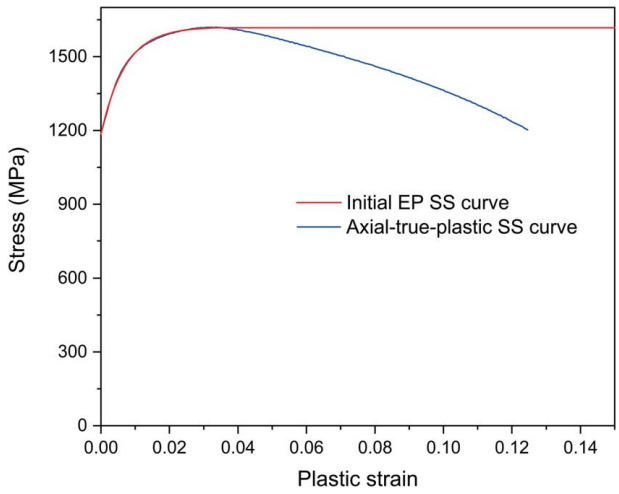

Fig. 6 Initially guessed EP SS curve prepared by fitting the pre-necking part of the axial-true SS curve in Fig. 5(*b*) using the Voce model

Figure 7(*c*) compares the finally extracted EP SS curve (Fig. 7(*b*), $j = 7$) with the plastic part of the axial-true SS curve (Fig. 5(*b*)) measured solely using the extensometer and load cell. In Fig. 7(*c*), a number of points as follows are noteworthy. First of all, the overall discrepancy of the two curves including the final (fracture) strain values on the two curves clearly illustrates the reward and necessity of extracting the EP SS curve from the tensile test of a necking material, especially via the proposed algorithm and presented method of necking initiation.

Second, the true SS curve in Fig. 7(*c*) shows apparent softening after the maximum stress where necking is initiated. Such apparent softening of the true SS curve appears because, in the post-necking regime, the calculated cross-sectional area (A) of the "cylindrical" specimen inputted to Eq. (S3) available in the (Supplemental Materials on the ASME Digital Collection) was overestimated as compared with the actual cross-sectional area of the neck where plastic deformation mostly occurs. This resulted in the underestimation of the true stress calculated using Eq. (S3). However, the extracted EP SS curve from the investigated specimen via the presented method (Fig. 7(*c*)) never exhibits such strain (work) softening but strain hardening is actually observed up to fracture. Therefore, the true SS curve of a necking material determined using the conventional method (using the foregoing equation) should not be used for the purpose of judging strain softening or hardening unless the EP SS curve is precisely determined via a reliable method such as the presented method here.

The third point is that the shape of the extracted EP SS curve ($j = 7$) is unique, and thus, the mathematical modeling of the extracted EP SS curve is challenging. There may be a limit in fitting the solution curve ($j = 7$) by controlling the parameter values of a constitutive model unless the model is complicated with an overly large number of parameters. This point indicates the importance of the EP SS curve extraction without assuming a constitutive model, as was done here.

Finally, focusing on the pre-necking part of the curves in Fig. 7(*c*), two curves are reasonably consistent in the initial plastic deformation regime, which indicates the reliability of the employed specimen geometry (Fig. 4(*a*)) in measuring the early stage of the EP SS curve via the axial-true SS curve. However, they differed before reaching the necking point (maximum point in the axial-true plastic SS curve). Therefore, it is desirable to apply our algorithm from the yield point especially for the employed specimen geometry here rather than from the necking point. There is no harm in verifying (or correcting) the measured axial-true SS curve from the yield point.

Figure 8 presents the change in error value with the progress of FEA iterations (index j) when different combinations of U_f and U_r were employed for the regimes of $F_{ratio} \leq 1$ and >1. As can be observed in Fig. 8, for the considered target data here (Fig. 7(*a*)), different combinations of U_f and U_r did not yield an apparent difference in the solution-approaching speed or characteristic. There is no physics-based principle about which of the update factors (U_f or U_r) will update the stress more properly to make the $F_{ratio}(=F_{sim}/F_{exp})$ value obtained in the next FEA cycle closer to unity. The appropriateness of the update factor may depend on the experimental data, the initially guessed EP SS curve, and also on the moment of stress update (indices i and j) during the iterative FEA process. Elucidating the influence of the $U_f - U_r$ combination on the solution-approaching characteristics as in Fig. 8 may require a test of their capability using more versatile data.

4.5 Effect of Mesh Size on the Extracted EP SS Curve

4.5.1 Initiating Necking in Experiment. In the standard tensile test (experiment) using a circular bar specimen, the chance of necking at the specimen center is not high; it can occur anywhere in the gauge part due to material flaws. Although not explicitly specified in the literature, in the practice of experiments, machining the diameter of the specimen center to be minutely smaller than the rest of the gage part (introducing a kind of geometric flaw) prevents

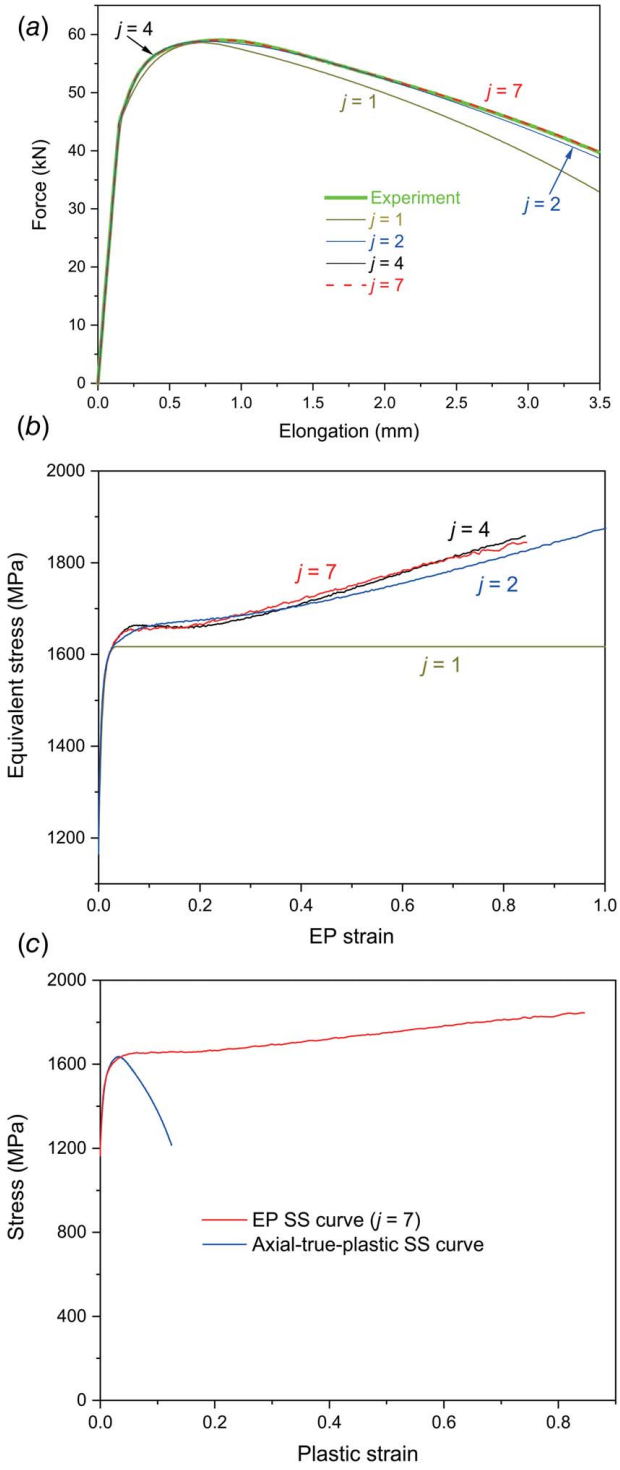

Fig. 7 Evolution of the (*a*) force–elongation and (*b*) EP SS curves with FEA iterations (index j) when U_f and U_r were employed to U in Eq. (1) when $F_{ratio} \leq 1$ and >1, respectively. The results from $j = 3$, 5, and 6 are intentionally undrawn to avoid complexity. (*c*) Comparison of the finally extracted EP SS curve ($j = 7$) with the plastic part of the axial-true SS curve in Fig. 5(*b*).

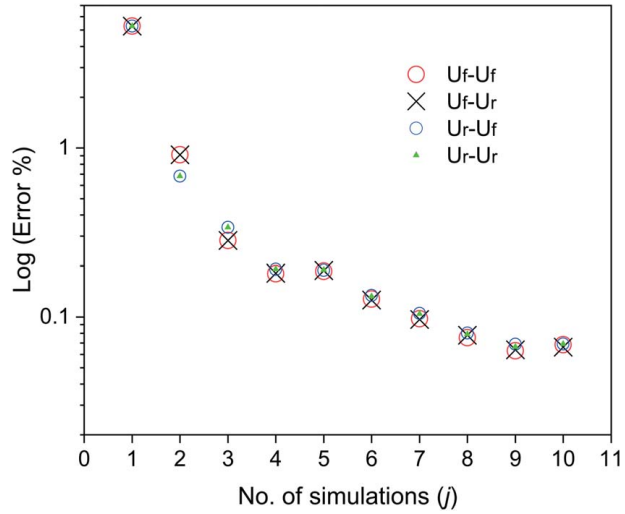

Fig. 8 Evolutions of the error value with the progress of FEA iterations (index *j*) when different combinations of U_f and U_r were employed for the regimes of $F_{ratio} \leq 1$ and >1

the sacrifice of unnecessarily many specimens in obtaining necking at the specimen center.

4.5.2 Initiating Necking in Finite Element Simulation. In the FE simulation of a cylinder model receiving tension along the axial direction, a constraint on the radial contraction at the cylinder ends results in a relatively higher degree of radial contraction at the specimen center, which fosters neck initiation there. Conversely, a purely cylindrical FE model without such an end constraint hardly results in necking (provided the FE simulation is rigorous without any truncation errors) because the whole cylinder volume is in a perfectly homogeneous stress state, and thus, there is no reason the stress at a certain point is higher than that at any other material points. This numerical phenomenon (no necking in a cylinder model without any radial constraint at the ends) was observed not only for a work-hardening material [54] but also for the materials satisfying the Considère condition during plastic deformation [55,56].

For an FE model of the tensile specimen (with grip, tapered, and gage parts), the radial contraction at the ends of the gage part is automatically constrained to some degree due to the presence of the tapered and grip parts, because the latter parts are thicker than the gage part. However, the contribution of the foregoing constraint to necking at the specimen center should diminish with gage-part length. A more certain method of stably triggering necking at the specimen center of the FE model is artificially introducing a geometrical flaw such as a slightly reduced diameter at the specimen center [57–60] (or a slightly reduced thickness for a rectangular bar specimen [61]).

4.5.3 Initiating Necking in Inverse Method Studies. In the inverse method studies for extracting the EP SS curve via iterative FE simulations and related studies, nevertheless, geometrically perfect models of tensile specimens (i.e., without any geometric flaws) [19–23,25–47] or even purely cylindrical FE models (without any end constraint) [24,48] were employed. In the majority of the inverse studies utilizing the geometrically perfect models of tensile specimens [19–23,25–34,41–47], simply finer (biased) meshes were employed at the specimen center region and necking was observed there. According to Refs. [19] and [42], the purpose of employing the finer meshes at the specimen center region was initiating necking there. However, although the fine meshes are necessary to flexibly describe the deformed shape of the neck region, the mesh size control itself is undesirable (inefficient) as a mean to stably induce necking in geometrically perfect models of tensile specimens. It is because, if there is a numerical truncation error in FEA, necking can be initiated not only in the fine meshes but also in the coarse ones [62]. Under the above circumstances, to the best of our knowledge, none of the inverse method studies [19–47] (which employed the geometrically perfect FE models) explicitly presented the data illustrating the

effect of mesh size on the finally extracted EP SS curve, probably because of the limitation in stably initiating necking over a range of mesh sizes in geometrically perfect FE models.

4.5.4 Mesh Size Sensitivity to Extracted EP SS Curve. In this study, necking was stably initiated at the specimen center in the simulations as well as in the experiments because a slightly tapered geometry was employed around the specimen center. Because necking was stably initiated here, a mesh-size sensitivity test could be carried out successfully from the viewpoint of achieving a converged EP SS curve after the iterative FEA process according to the proposed algorithm. The result is presented in Fig. 9, where n denotes the number of meshes along the r direction in the FE model (see Fig. 4(*b*) for $n = 32$).

In Fig. 9, each EP SS curve (obtained using different mesh sizes) was extracted as the solution curve after seven FE simulations according to the proposed algorithm when the error of the simulated force–elongation curve was less than the arbitrarily predefined level here (0.1%). In Fig. 9, as the number of meshes increases (mesh size decreases), the fracture EP strain increases and the EP SS curve shifts upward, especially near the fracture strain, to reach a converged curve. This result indicates that, although the error of the simulated force–elongation curve using a given mesh size (e.g., $n = 4$–8) is less than 0.1% and thus the inputted EP SS curve was determined to be the solution curve at a given mesh size, the extracted EP SS curve can be notably different from the converged solution curve at a sufficiently fine mesh size (e.g., $n = 32$–128). Figure 9 illustrates the importance of verifying the convergence of the finally extracted solution curve over a range of mesh sizes.

From the result in Fig. 9, the mesh size for $n = 32$ was employed here, which is illustrated in Fig. 4(*b*). When a qualified mesh (e.g., $n = 32$–128) was employed, the simulated final diameter of the neck was reasonably consistent with the experiment (Fig. 4(*c*)). One may select a finer mesh size of $n = 64$ or 128 with the investment of computation time.

5 Further Discussion

5.1 Fracture Strain of Necking Material in Tensile Test. To simulate the fracture behavior of ductile solids and structures, an appropriate fracture model needs to be employed in addition to the constitutive relationship. To calibrate a fracture model, the values of $\bar{\varepsilon}_f$ need to be quantified for versatile types of specimens under various stress states (triaxiality, Lode parameter, etc. [63]).

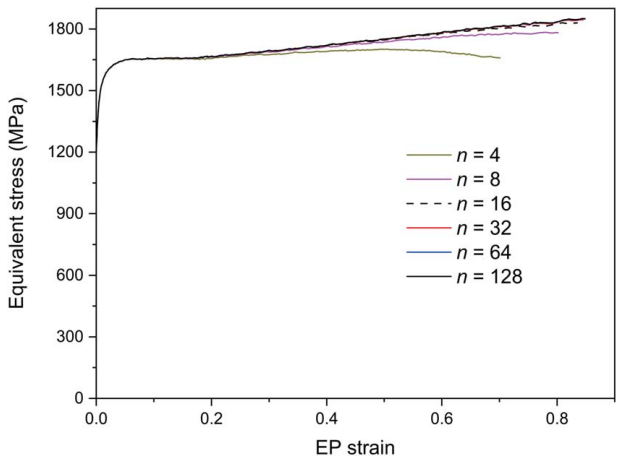

Fig. 9 Result of the mesh size sensitivity test from the viewpoint of obtaining the converged EP SS curve via the iterative FE simulations. The update factors of U_f and U_r were employed to U in Eq. (1) when $F_{ratio} \leq 1$ and >1, respectively.

The process of $\bar{\varepsilon}_f$ value quantification for a given specimen type is a reverse engineering process, where repeated FE simulations are generally carried out by assuming a range of $\bar{\varepsilon}_f$ values for the constant EP strain model [63]. In such a case, the infallible EP SS curve (constitutive relationship) should be inputted to the FE solver. However, the EP SS curve of a necking material is generally unavailable in advance.

In Fig. 7(*a*), the specimen elongation was controlled in FEA up to an experimental fracture elongation value of 3.49 mm. It is thus reasonable to regard the final strain of the extracted EP SS curve (for $j = 7$) in Fig. 7(*c*) as the $\bar{\varepsilon}_f$ value (0.85 for the investigated specimen). More desirably, the EP strain of the neck element (nearest to the origin) can be outputted when the elongation reaches the value at fracture (3.49 mm here). In this way, we quantified the $\bar{\varepsilon}_f$ value simultaneosly with extracting the EP SS curve. Unlike the conventional method of determining the fracture strain, we neither employed any fracture model nor assumed any fracture strain values in the FE simulations. Furthermore, the determined fracture strain value here is the converged value over a range of mesh sizes.

5.2 Reference for EP SS Curve at High Strain Rates. The necessity of simulating many high-strain-rate phenomena of ductile solids and structures is steadily increasing [64,65], which requires information on the strain-rate dependency of the EP SS curve. To quantify the degree of strain-rate dependency, infallible EP SS curves measured at both (i) quasi-static and (ii) high strain rates [66–68] need to be compared. The extracted EP SS curve here in a quasi-static strain rate can serve as the reliable comparison standard for high-strain-rate EP SS curves.

6 Conclusion

The method of extracting the EP SS curve of a necking material without assuming a constitutive model was critically reviewed, which traced the force–elongation curve of the tensile test via iterative FE simulations. We then proposed a new algorithm, that is suitable for a general-purpose FE solver because the stresses at all elongation steps are updated after each FEA cycle in the post-processing stage (unlike the stress update loop at a given elongation step in previous studies). The proposed algorithm employs a new base stress in the stress update equation and combines a newly introduced fraction-based stress update factor with the existing ratio-based one. In the FE simulation and experiment, a slightly tapered geometry was employed around the specimen center to stably initiate necking there. The proposed algorithm and mentioned necking initiation method were applied to the standard tensile test of a steel material using an axisymmetric specimen. Because yielding occurred stably in simulations at the specimen center for a range of mesh sizes, we successfully verified the convergence of the solution curve with the mesh size. The EP SS curve of a high-strength steel material was extracted in the proposed way up to an EP strain of 0.85 with average strain intervals of approximately 2.5 mili-strain. The error values were less than 0.2 and 0.1% after four and seven FE simulations, respectively. The presented algorithm and necking initiation method in simulation can also be used for simultaneously quantifying the fracture EP strain of a necking material in the tensile test. The extracted EP SS curve here in a quasi-static strain rate can serve as the reliable comparison standard for high-strain-rate EP SS curves.

Acknowledgment

The authors thank Hyunsuk Cho, Jaehyuk Lee, and Junmoo Lee for their technical support.

Funding Data

- Agency for Defense Development (Contract No. UE201106GD), funded by Korea Government (Defense Acquisition Program Administration).

Conflict of Interest

There are no conflicts of interest.

Data Availability Statement

The datasets generated and supporting the findings of this article are obtainable from the corresponding author upon reasonable request.

Nomenclature

e = engineering strain (axial quantity)
i = index of predefined elongation step δ^i (or ε^i)
j = index of FEA iteration
s = engineering stress (axial quantity)
A = current cross-sectional area
L = current cylinder (specimen) length
A^i = step of minimum cross-sectional area (A) at δ^i
A_o = initial cross-sectional area
F_{ratio} = F_{sim}/F_{exp}
F_{sim} = simulated axial force via FEA of tensile test
L_o = initial cylinder (specimen) length
$F_{exp}(=F)$ = measured axial force in tensile test
δ = current elongation ($\delta = L - L_o$)
δ^i = predefined elongation step ($\delta^i = \delta^i_{exp} = \delta^i_{sim}$)
ε = axial-true plastic strain determined under the assumption of incompressible and uniform deformation
ε^i = predefined ε step. Or ε at a predefined δ^i step
$\bar{\varepsilon}$ = equivalent-plastic (EP) strain in the neck region (average, representative, or largest value)
$\bar{\varepsilon}^i$ = $\bar{\varepsilon}$ at a predefined step δ^i (or ε^i)
$\bar{\varepsilon}_f$ = fracture equivalent plastic strain
$\bar{\varepsilon}_{input}$ = inputted EP strain to FEA
$\bar{\varepsilon}_{output}$ = outputted EP strain from FEA
σ = axial-true stress determined under the assumption of incompressible and uniform deformation
σ^i = σ at a predefined step (δ^i or ε^i)
$\bar{\sigma}$ = equivalent stress in the neck region (average, representative, or largest value)
$\bar{\sigma}^i$ = $\bar{\sigma}$ at a predefined step δ^i (or ε^i)
$\bar{\sigma}_{input}$ = inputted equivalent stress to FEA
$\bar{\sigma}_{output}$ = outputted equivalent stress from FEA

References

[1] Kim, N.-H., 2015, *Introduction to Non-Linear Finite Element Analysis*, Springer, New York.
[2] Borja, R. I., 2013, *Plasticity*, Springer, Berlin, Heidelberg.
[3] Halim, S. T., and Ng, E.-G., 2023, "A Unique Method to Determine Ferrite and Martensite Phase Stress–Strain Curve for Manufacturing Process," ASME J. Eng. Mater. Technol., **145**(2), p. 021003.
[4] Shin, H., Ju, Y., Choi, M. K., and Ha, D. H., 2022, "Flow Stress Description Characteristics of Some Constitutive Models at Wide Strain Rates and Temperatures," Technologies, **10**(2), p. 52.
[5] Voyiadjis, G. Z., Hoseini, S. H., and Farrahi, G. H., 2013, "A Plasticity Model for Metals With Dependency on All the Stress Invariants," ASME J. Eng. Mater. Technol., **135**(1), p. 011002.
[6] Ito, K., and Arai, M., 2020, "Expanding Cavity Model Combined With Johnson–Cook Constitutive Equation for the Dynamic Indentation Problem," ASME J. Eng. Mater. Technol., **142**(2), p. 021005.
[7] Shin, H., and Kim, J.-B., 2010, "A Phenomenological Constitutive Equation to Describe Various Flow Stress Behaviors of Materials in Wide Strain Rate and Temperature Regimes," ASME J. Eng. Mater. Technol., **132**(2), p. 021009.
[8] Buchely, M. F., Wang, X., Van Aken, D. C., O'Malley, R. J., Lekakh, S., and Chandrashekhara, K., 2019, "The Use of Genetic Algorithms to Calibrate Johnson–Cook Strength and Failure Parameters of AISI/SAE 1018 Steel," ASME J. Eng. Mater. Technol., **141**(2), p. 021012.
[9] Kirka, M. M., and Neu, R. W., 2019, "Crystal Viscoplasticity of a Ni-Base Superalloy in the Aged State," ASME J. Eng. Mater. Technol., **141**(1), p. 011003.
[10] La Rosa, G., Risitano, A., and Mirone, G., 2003, "Postnecking Elastoplastic Characterization: Degree of Approximation in the Bridgman Method and Properties of the Flow-Stress/True-Stress Ratio," Metall. Mater. Trans., **34**(3), pp. 615–624.
[11] Gromada, M., Mishuris, G., and Öchsner, A., 2011, *Correction Formulae for the Stress Distribution in Round Tensile Specimens at Neck Presence*, Springer Science Business Media.
[12] Majzoobi, G. H., Fariba, F., Pipelzadeh, M. K., and Hardy, S. J., 2014, "A New Approach for the Correction of Stress–Strain Curves After Necking in Metals," J. Strain Anal. Eng. Des., **50**(2), pp. 125–137.
[13] Mirone, G., 2004, "A New Model for the Elastoplastic Characterization and the Stress–Strain Determination on the Necking Section of a Tensile Specimen," Int. J. Solids Struct., **41**(13), pp. 3545–3564.
[14] Tu, S., Ren, X., He, J., and Zhang, Z., 2018, "A Method for Determining Material's Equivalent Stress-Strain Curve With Any Axisymmetric Notched Tensile Specimens Without Bridgman Correction," Int. J. Mech. Sci., **135**, pp. 656–667.
[15] Sławomir, S., and Robert, C., 2023, "A New Approach for Evaluation True Stress–Strain Curve From Tensile Specimens for DC04 Steel With Vision Measurement in the Post-Necking Phases," Materials, **16**(2), p. 558.
[16] Yuan, W. J., Zhang, Z. L., Su, Y. J., Qiao, L. J., and Chu, W. Y., 2012, "Influence of Specimen Thickness With Rectangular Cross-Section on the Tensile Properties of Structural Steels," Mater. Sci. Eng. A, **532**, pp. 601–605.
[17] Choung, J. M., and Cho, S. R., 2008, "Study on True Stress Correction From Tensile Tests," Mech. Sci. Tech., **22**(6), pp. 1039–1051.
[18] Scheider, I., Brocks, W., and Cornec, A., 2004, "Procedure for the Determination of True Stress–Strain Curves From Tensile Tests With Rectangular Cross-Section Specimens," ASME J. Eng. Mater. Technol., **126**(1), pp. 70–76.
[19] Ling, Y., 1996, "Uniaxial True Stress-Strain After Necking," AMP Tech., **5**, pp. 37–48.
[20] Wang, Y.-Z., Li, G.-Q., Wang, Y.-B., and Lyu, Y.-F., 2021, "Simplified Method to Identify Full von Mises Stress-Strain Curve of Structural Metals," J. Construct. Steel Res., **181**, p. 106624.
[21] Beltramo, M., Scapin, M., and Peroni, L., 2023, "An Advanced Post-Necking Analysis Methodology for Elasto-Plastic Material Models Identification," Mater. Design, **230**, p. 111937.
[22] Chen, J., Guan, Z., and Yang, C., 2020, "Inverse Determination of the Flow Curve in Large Range of Strains for Cylindrical Tensile Specimen," Proc. Inst. Mech Eng. Part C: Mech. Eng. Sci., **234**(11), pp. 2256–2265.
[23] Cabezas, E. E., and Celentano, D. J., 2004, "Experimental and Numerical Analysis of the Tensile Test Using Sheet Specimens," Finite Elem. Anal. Des., **40**(5–6), pp. 555–575.
[24] Joun, M. S., Eom, J. G., and Lee, M. C., 2008, "A New Method for Acquiring True Stress–Strain Curves Over a Large Range of Strains Using a Tensile Test and Finite Element Method," Mech. Mater., **40**(7), pp. 586–593.
[25] Koc, P., and Štok, B., 2004, "Computer-Aided Identification of the Yield Curve of a Sheet Metal After Onset of Necking," Comput. Mater. Sci., **31**(1), pp. 155–168.
[26] Joun, M. S., Razali, M. K., Jee, C. W., Byun, J. B., Kim, M. C., and Kim, K. M., 2022, "A Review of Flow Characterization of Metallic Materials in the Cold Forming Temperature Range and Its Major Issues," Mater., **15**(8), p. 2751.
[27] Kweon, H. D., Kim, J. W., Song, O., and Oh, D., 2021, "Determination of True Stress-Strain Curve of Type 304 and 316 Stainless Steels Using a Typical Tensile Test and Finite Element Analysis," Nucl. Eng. Tech., **53**(2), pp. 647–656.
[28] Hyun, H. C., Kim, M., Bang, S., and Lee, H., 2014, "On Acquiring True Stress–Strain Curves for Sheet Specimens Using Tensile Test and FE Analysis Based on a Local Necking Criterion," Mater. Res., **29**(5), pp. 695–707.
[29] Razali, M. K., Joun, M. S., and Chung, W. J., 2021, "A Novel Flow Model of Strain Hardening and Softening for Use in Tensile Testing of a Cylindrical Specimen at Room Temperature," Materials, **14**(17), p. 4876.
[30] Byun, J. B., Jee, C. W., Lee, K. H., and Joun, M. S., 2023, "General Blending Approach of Fundamental Cold Flow Models for an Almost Complete Cold Flow Model in Terms of Tensile Test," Steel Res. Int., **94**(9), p. 2200540.
[31] Zhao, K., Wang, L., Chang, Y., and Yan, J., 2016, "Identification of Post-Necking Stress–Strain Curve for Sheet Metals by Inverse Method," Mech. Mater., **92**, pp. 107–118.
[32] Jones, C. A., 2019, "A Method for Developing the True Stress–Strain Relationship for Structural Steels Based on Tension Coupon Tests," Ph.D. Thesis, The University of Texas, Austin, TX.
[33] Marth, S., Djebien, S., Kajberg, J., and Häggblad, H.-Å., 2021, "Stepwise Modelling Method for Post Necking Characterisation of Anisotropic Sheet Metal," Model. Simul. Mater. Sci. Eng., **29**(8), p. 085001.
[34] Pham, Q.-T., Oh, S.-H., and Kim, Y.-S., 2018, "An Efficient Method to Estimate the Post-Necking Behavior of Sheet Metals," Adv. Manuf. Technol., **98**(9–12), pp. 2563–2578.
[35] Neggers, J., Hoefnagels, J. P. M., Geers, M. G. D., Hild, F., and Roux, S., 2015, "Time-Resolved Integrated Digital Image Correlation," Int. J. Numer. Meth. Eng., **103**(3), pp. 157–182.
[36] Kim, J.-H., Serpantié, A., Barlat, F., Pierron, F., and Lee, M.-G., 2013, "Characterization of the Post-Necking Strain Hardening Behavior Using the Virtual Fields Method," Int. J. Solids Struct., **50**(24), pp. 3829–3842.
[37] Kajberg, J., and Lindkvist, G., 2004, "Characterisation of Materials Subjected to Large Strains by Inverse Modelling Based on In-Plane Displacement Fields," Int. J. Solid Struct., **41**(13), pp. 3439–3459.

[38] Ilg, C., Liebold, C., Sreenivasa, V., Haufe, A., Karadogan, C., and Liewald, M., 2023, "Displacement Based Simulation and Material Calibration Based on Digital Image Correlation Part II—Application," IOP Conf. Ser.: Mater. Sci. Eng., **1284**(1), p. 012056.
[39] Gerbig, D., Bower, A., Savic, V., and Hector, L. G., 2016, "Coupling Digital Image Correlation and Finite Element Analysis to Determine Constitutive Parameters in Necking Tensile Specimens," Int. J. Solid Struct., **97–98**, pp. 496–509.
[40] Gross, A. J., and Ravi-Chandar, K., 2015, "On the Extraction of Elastic–Plastic Constitutive Properties From Three-Dimensional Deformation Measurements," ASME J. Appl. Mech., **82**(7), p. 071013.
[41] Zhano, K. S., and Li, Z. H., 1994, "Numerical Analysis of the Stress-Strain Curve and Fracture Initiation for Ductile Material," Eng. Frac. Mech., **49**(2), pp. 235–241.
[42] Chu, S. J., 2011, "True Stress–True Strain Curves Obtained by Simulating Tensile Tests Using Finite Element Program (In Korean)," Trans. Korean Soc. Mech. Eng. A, **35**(10), pp. 25–31.
[43] Kamaya, M., and Kawakubo, M., 2011, "A Procedure for Determining the True Stress–Strain Curve Over a Large Range of Strains Using Digital Image Correlation and Finite Element Analysis," Mech. Mater., **43**(5), pp. 243–253.
[44] Wang, Y. D., Xu, S. H., Ren, S. B., and Wang, H., 2016, "An Experimental-Numerical Combined Method to Determine the True Constitutive Relation of Tensile Specimens After Necking," Adv. Mater. Sci. Eng., **2016**, p. 6015752.
[45] Mei, H., Lang, L., Liu, K., and Yang, X., 2018, "Evaluation Study on Iterative Inverse Modeling Procedure for Determining Post-Necking Hardening Behavior of Sheet Metal at Elevated Temperature," Metals, **8**(12), p. 1044.
[46] Tao, H., Zhang, N., and Tong, W., 2009, "An Iterative Procedure for Determining Effective Stress–Strain Curves of Sheet Metals," Int. J. Mech. Mater. Des., **5**, pp. 13–27.
[47] Tardif, N., and Kyriakides, S., 2012, "Determination of Anisotropy and Material Hardening for Aluminum Sheet Metal," Int. J. Solid Struct., **49**(25), pp. 3496–3506.
[48] Joun, M., Choi, I., Eom, J., and Lee, M., 2007, "Finite Element Analysis of Tensile Testing With Emphasis on Necking," Comput. Mater. Sci., **41**(1), pp. 63–69.
[49] Kang, B. S.-J., Yao, Z., and Barbero, E. J., 2006, "Post-Yielding Stress-Strain Determination Using Spherical Indentation," Mech. Adv. Mater. Struct., **13**(2), pp. 129–138.
[50] Lee, J.-H., Shin, H., Kim, J.-B., Kim, J.-Y., Park, S.-T., Kim, G.-L., and Oh, K.-W., 2019, "Determination of the Flow Stress–Strain Curve of Aluminum Alloy and Tantalum Using the Compressive Load–Displacement Curve of a Hat-Type Specimen," ASME J. Appl. Mech., **86**(3), p. 031012.
[51] Ehlers, S., and Varsta, P., 2009, "Strain and Stress Relation for Non-Linear Finite Element Simulations," Thin-Walled Struct., **47**(11), pp. 1203–1217.
[52] Smith, M., 2009, ABAQUS/Standard User's Manual, version 6.9, Dassault Systèmes Simulia Corp., Providence.
[53] Matweb, Material Property Data, 2023, https://www.matweb.com/search/QuickText.aspx?SearchText=4340, Accessed October 30, 2023.
[54] Le Van, A., and Le Grognec, P., 2001, "Modeling and Numerical Computation of Necking in Round Bars Using a Total Lagrangian Elastoplastic Formulation," Comput. Model. Eng. Sci., **2**(1), pp. 63–72.
[55] Kim, H. S., Kim, S. H., and Ryu, W.-S., 2005, "Finite Element Analysis of the Onset of Necking and the Post-Necking Behaviour During Uniaxial Tensile Testing," Mater. Trans., **46**(10), pp. 2159–2163.
[56] Kolwankar, S., Kanvinde, A., Kenawy, M., and Kunnath, S., 2017, "Uniaxial Nonlocal Formulation for Geometric Nonlinearity–Induced Necking and Buckling Localization in a Steel Bar," J. Struct. Eng., **143**(9), p. 04017091.
[57] Nilsson, K., 2001, "Effects of Inertia on Dynamic Neck Formation in Tensile Bars," Eur. J. Mech. A/Solids, **20**(5), pp. 713–729.
[58] Shaw, J. A., and Kyriakides, S., 1997, "Initiation and Propagation of Localized Deformation in Elasto-Plastic Strips Under Uniaxial Tension," Int. J. Plasticity, **13**(10), pp. 837–871.
[59] Tomita, Y., Adachi, T., and Sik, P. S., 1997, "Computational Simulation of Three-Dimensional Neck Propagation in Polymeric Specimens Under Tension and Hybrid Identification of Constitutive Equation," Int. J. Mech. Sci., **39**(8), pp. 913–923.
[60] Brünig, M., 1998, "Numerical Analysis and Modeling of Large Deformation and Necking Behavior of Tensile Specimens," Finite Elem. Anal. Des., **28**(4), pp. 303–319.
[61] van den Boogaard, A. H., and Huetink, J., 2003, "Prediction of Sheet Necking With Shell Finite Element Models," Proceedings of the ESAFORM 2003: 6th International ESAFORM Conference on Material Forming, Salerno, Italy, Apr. 28–30, 2003, pp. 1–4.
[62] Panchal, M., Raval, H. K., and Narasimhan, K., 2013, "Analysis of Various Necking Criteria in Sheet Metal Forming," Technical Report No. 8-13\TR \NECKSMF\V1, National Centre for Aerospace Innovation and Research (NCAIR), IIT-Bombay, India. http://ncair.in/pdf/Reports/TR-2013-02_Manan, Raval_&_Narsimhan.pdf.
[63] Wierzbicki, T., Bao, Y., Lee, Y.-W., and Bai, Y., 2005, "Calibration and Evaluation of Seven Fracture Models," Int. J. Mech. Sci., **47**(4-5), pp. 719–743.
[64] Shin, H., Lee, H.-J., Yoo, Y.-H., and Lee, W., 2004, "A Determination Procedure for Element Elimination Criterion in Finite Element Analysis of High-Strain-Rate Impact/Penetration Phenomena," JSME Int. J. Ser. A, **47**(1), pp. 35–41.
[65] Thomas, G. O., and Oakley, G. L., 2020, "A Study of the Strain Response of Stainless Steel 304 to Extreme Uniform Instantaneous Explosion Pressure Loads," ASME J. Eng. Mater. Technol., **142**(1), p. 011007.
[66] Shin, H., and Kim, J. B., 2019, "Evolution of Specimen Strain Rate in Split Hopkinson Bar Test," Proc. Inst. Mech. Eng. Part C: J. Mech. Eng. Sci., **233**(13), pp. 4667–4687.
[67] Shin, H., 2022, "Sound Speed and Poisson's Ratio Calibration of (Split) Hopkinson Bar via Iterative Dispersion Correction of Elastic Wave," ASME J. Appl. Mech., **89**(6), p. 061007.
[68] Shin, H., 2023, "Calibration of Bar Properties, Measured Strain, and Impact Velocity in a Bar Impact Test," Mech. Adv. Mater. Struct.,